

The Recurrent Nova T Pyx: Distance and Remnant Geometry from Light Echoes

J. L. Sokoloski¹, Arlin P. S. Crotts, and Helena Uthas²

Columbia Astrophysics Laboratory, Columbia University, 550 West 120th Street, New
York, NY 10027, USA

and

Stephen Lawrence³

Department of Physics and Astronomy, Hofstra University, Hempstead, NY 11549, USA

Received _____; accepted _____

ABSTRACT

The recurrent nova T Pyxidis (T Pyx) is well known for its small binary separation, its unusually high luminosity in quiescence, and the spectacular Hubble Space Telescope (*HST*) images of its surrounding remnant. In 2011 April, T Pyx erupted for the first time since 1966. Here we describe *HST* observations in late 2011 of a transient reflection nebula around the erupting white dwarf (WD). Our observations of this light echo in the pre-existing remnant show that it is dominated by a clumpy ring with a radius of about $5''$ and an inclination of $30^\circ - 40^\circ$, with the eastern edge tilted toward the observer. The delay times between the direct optical light from the central source, and the scattering of this light from dust in several clumps with the same foreground distance as the central source, give a distance to T Pyx of 4.8 ± 0.5 kpc. Given past evidence from two-dimensional optical spectra that the remnant contains a shell-like component, it must actually consist of a ring embedded within a quasi-spherical shell. The large distance of 4.8 kpc supports the contention that T Pyx has an extraordinarily high rate of mass transfer in quiescence, and thus that nova explosions themselves can enhance mass loss from a donor star, and reduce the time between eruptions in a close binary.

Subject headings: accretion, accretion disks — novae, cataclysmic variables — stars: evolution — stars: imaging — stars: individual (T Pyxidis) — stars: winds, outflows

1. Introduction

During a nova eruption, material is explosively ejected from the surface of an accreting white dwarf (WD). Nova explosions thus alter the evolution of the WD. Copious emission from novae also probably influences the companion star and the host cataclysmic variable (CV; e.g., Patterson et al. 2012). The companion star, in turn, must modify the shape of the ejecta. However, the way in which the exploding WD and the donor star disturb one another — e.g., the degree to which the close companion generates asymmetry in the remnant, the mechanism of such shaping, and the affect of the outburst on the mass transfer rate — are poorly understood.

T Pyx is an unusual CV that from years 1890 and 1966 suffered recurrent nova eruptions roughly every 20 years. Compared to other CVs with similar orbital periods, T Pyx has a much higher accretion rate, and hence luminosity (e.g., Patterson et al. 1998). It can also have a high ejecta mass for a recurrent nova (Nelson et al. 2013; Patterson et al. 2013). Both the high luminosity and frequent nova eruptions may be part of a self-perpetuating cycle in which nova eruptions trigger enhanced mass-loss from the donor star, as first proposed by Knigge et al. (2000). Previous images of the remnant around T Pyx in $H\alpha$ and [NII] line emission revealed thousands of knots within about $6''$ of the central binary and a halo possibly extending out to $10''$ — resulting from multiple recent nova eruptions (Shara et al. 1989, 1997; Schaefer et al. 2010). The most recent eruption was discovered on 2011 April 14.29 (Waagen 2011). Because T Pyx is the only nova confirmed to have erupted within a pre-existing remnant (e.g., Shara et al. 1989, 1997; Schaefer et al. 2010), it provides a rare opportunity to examine the ejecta from a nova using a light echo.¹

¹N Sagittarii 1936 may have also produced such an echo (Swope 1940). The light and ionization echoes from GK Persei, V458 Vulpeculae, and V838 Monocerotis probed either surrounding planetary nebulae or pre-existing circumstellar dust from an unusual type of

Below, we describe how Hubble Space Telescope (*HST*) observations of the light echo around T Pyx reveal: 1) how much the companion has shaped the remnant; and 2) T Pyx’s distance, with implications for understanding how novae influence binary stellar evolution.

2. Observations and Data Reduction

HST observed T Pyx using the Wide Field Camera 3 (WFC3) nine times between 2011 July and 2012 May, and using the Space Telescope Imaging Spectrograph (STIS) with G430L and G750L low-resolution gratings and a slit width of 2'' three times between 2011 May and 2011 December (program 12448; see Table 1). To isolate the signal due primarily to scattering by dust, we selected four filters that exclude strong recombination lines: F225W (UV wide filter), FQ422M (blue continuum), F547M (Strömgren-*y*), and F600LP (long-pass). Every WFC3 observation included F547M exposures, which we refer to as *visual-light* observations.

To reduce the WFC3 images, we subtracted the point spread function (PSF) of the central source from 2011 July, and interpolated across small regions where charge was saturated due to PSF brightness and column bleeding. For F547M images, we define an angular distance from the central binary, θ_{bright} , as that within which residuals from the subtracted central-source PSF reduced sensitivity to the light echo. In 2011 July, θ_{bright} was greater than the size of most of the known remnant (approximately 6''). It decreased in later epochs as the central source faded.

stellar eruption (Bode et al. 2004; Wesson et al. 2008; Bond et al. 2003; Soker & Tylenda 2007).

Table 1. Log of HST observations

Epoch	Instru- ment	Date	Day ^a	Exp Time ^b	Apertures	Filters/ Gratings	Offset ^c (")	PA ^d (°)
1	STIS	2011-05-19	35.1	205.0	STIS-52X2	G750L	-1.229	61.05
			35.1	615.0	STIS-52X2	G750L	-1.229	61.05
			35.1	205.0	STIS-52X2	G430L	-1.229	61.05
			35.1	615.0	STIS-52X2	G430L	-1.229	61.05
			35.2	205.0	STIS-52X2	G750L	1.303	57.55
			35.2	615.0	STIS-52X2	G750L	1.303	57.55
			35.2	205.0	STIS-52X2	G430L	1.303	57.55
			35.2	615.0	STIS-52X2	G430L	1.303	57.55
			35.2	820.0	STIS-52X2	G750L	3.654	52.65
			35.2	820.0	STIS-52X2	G430L	3.654	52.65
2	STIS	2011-05-26	42.1	820.0	STIS-52X2	G750L	-4.341	67.85
			42.1	820.0	STIS-52X2	G430L	-4.341	67.85
3	WFC3	2011-07-08	85.7	300.0	UVIS-QUAD-SUB	FQ422M		
				500.0	UVIS2-2k2C-SUB	F547M		
				1197.0	UVIS2-2k2C-SUB	F225W		
4	WFC3	2011-09-19	158.7	300.0	UVIS-QUAD-SUB	FQ422M		
				500.0	UVIS2-2k2C-SUB	F547M		
				800.0	UVIS2-2k2C-SUB	F225W		
				40.0	UVIS2-2k2C-SUB	F600LP		
5	WFC3	2011-09-26	165.1	1125.0	UVIS-QUAD-SUB	FQ422M		
				900.0	UVIS2-2k2C-SUB	F547M		
6	WFC3	2011-11-16	215.8	1125.0	UVIS-QUAD-SUB	FQ422M		
				900.0	UVIS2-2k2C-SUB	F547M		

Table 1—Continued

Epoch	Instru- ment	Date	Day ^a	Exp Time ^b	Apertures	Filters/ Gratings	Offset ^c (")	PA ^d (°)
7	WFC3	2011-11-25	224.8	300.0	UVIS-QUAD-SUB	FQ422M		
				500.0	UVIS2-2k2C-SUB	F547M		
				800.0	UVIS2-2k2C-SUB	F225W		
				40.0	UVIS2-2k2C-SUB	F600LP		
8	STIS	2011-12-05	235.6	830.0	STIS-52X2	G750L	2.000	-119.35
				830.0	STIS-52X2	G430L	2.000	-119.35
				830.0	STIS-52X2	G750L	-2.000	-91.35
				830.0	STIS-52X2	G430L	-2.000	-91.35
				830.0	STIS-52X2	G750L	-5.300	-109.35
				830.0	STIS-52X2	G430L	-5.300	-109.35
				830.0	STIS-52X2	G750L	4.500	-109.35
				830.0	STIS-52X2	G430L	4.500	-109.35
9	WFC3	2011-12-10	240.7	2490.0	UVIS2-2k2C-SUB	F547M		
10	WFC3	2012-01-22	282.8	5295.0	UVIS2-2k2C-SUB	F547M		
11	WFC3	2012-02-22	314.2	5295.0	UVIS2-2k2C-SUB	F547M		
12	WFC3	2012-05-21	403.4	5295.0	UVIS2-2k2C-SUB	F547M		

^aDays after $t_0 = \text{JD } 2455665.79$.

^bExposure time, in seconds.

^cOffset of the central source perpendicular to the center of the STIS slit, in the red-ward dispersion direction.

^dThe position angle of the slit, projected onto the sky, east of north.

To reduce the STIS spectra, we followed the standard CALSTIS pipeline within IRAF. We also manually removed the extensive “warm pixel” artifacts, cosmic rays and their charge-transfer tails through careful inspection of the three CR-SPLIT sub-exposures taken in each spectrum.

3. Results: Variable Ring of Emission

Between 2011 September and December (5 to 8 months after the eruption’s start), *HST*/WFC3 detected multiple transient patches of visual-light emission in a ring-like configuration around the central binary (see white arrows in Figure 1). We refer to this transient emission as an *echo* and justify this choice of terminology in §4. In 2011 July, the central source was too bright for echoes to be detectable at the location of the known remnant. In 2011 September, the echo was dominated by two swathes of emission $4''$ to $6''$ to the north and south of the central binary, respectively (see Figure 1; $4'' < \theta < 6''$, where θ is the angular distance from the central binary). By 2011 November, the echo had shifted dramatically — the brightest portion lay to the west of the central binary, with angular extent $\theta \lesssim 4''$, and an additional new patch of emission was present to the northwest of the central source. Several small patches of emission also remained to the north and south of the central binary, but at larger θ than in 2011 September. In 2011 December, the echo continued progressing west and to slightly larger θ , while fading overall. Virtually all of the visual echo had disappeared by 2012 January 22, within 10 months of the eruption’s start. *HST*/WFC3 detected no significant visual echo in 2012 March or May. *HST*/WFC3 also detected no extended structure through filters F225W or FQ422M during any epoch of this observing campaign, and only hints of a signal at the location of the visual echo with the

F600LP filter.² Figure 1 shows the visual echo traveling predominantly from east to west around an irregular, patchy partial ring.

In addition to the partial ring, *HST*/WFC3 detected several other clumps of reflecting material. Two small patches of visual emission appeared briefly to the southeast of the ring and central binary — one in 2011 September at $\theta \approx 12''$ and $PA \approx 130^\circ$, and one in 2011 November at $\theta \approx 10''$ and $PA \approx 137^\circ$. Given the low signal-to-noise level of the visual echoes, we cannot, however, place strong constraints on additional material outside roughly $\theta \approx 6''$. Inside the ring, a diffuse patch was present at $PA \approx 35^\circ$ in 2011 September. Therefore, between 2011 September and December, *HST* detected visual-light echoes from regions associated with most of the dominant features of the quiescent-state, $H\alpha$ -emitting remnant (as shown in, e.g., Shara et al. 1989; Schaefer et al. 2010).

The remnant’s spectrum was dominated by two emission lines: $H\alpha$ and [O III]. Although our spectroscopic observations in 2011 May, and two slit positions in 2011 December, furnished no useful information due to high background from the PSF of the bright central source, and a third slit position in 2011 December covered no obvious echo patches, the 2011 December slit position with an offset of $4.5''$ included the northwest echo region, from which we detected WFC3/visual-band emission on both 2011 November 15 and 2011 December 10. The long-wavelength (G750L) spectrum at this position revealed clear $H\alpha$ line emission with a complex profile most likely due to the distribution of material within the slit (Figure 2). In the short-wavelength spectrum (G430L), the most obvious signal was emission from [O III] $\lambda 5007\text{\AA}$. No strong emission lines appeared in the wavelength region to which the F547M filter is sensitive — consistent with the visual echo

²The lack of a F600LP exposure in 2011 July, and the corresponding lack of a high-quality empirical PSF at these wavelengths, prevented us from obtaining quantitative results for the red echo.

consisting of predominantly scattered continuum emission.

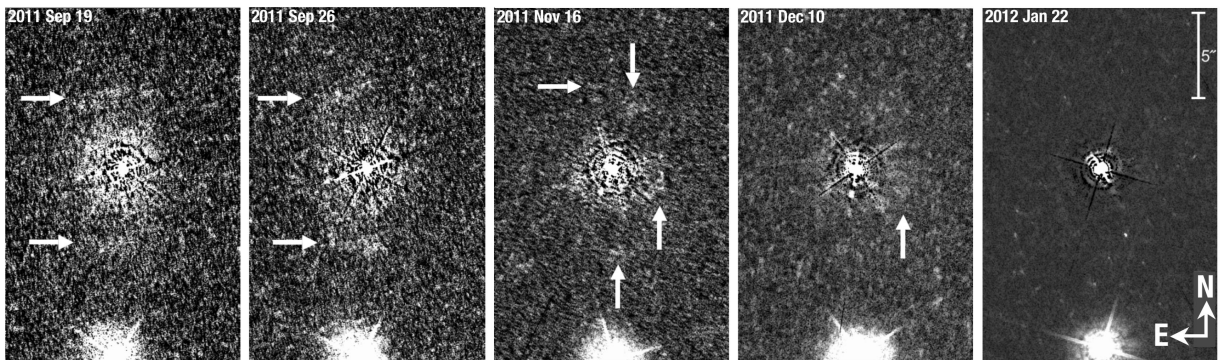


Fig. 1.— Series of *HST*/WFC3 images, from 2011 Sep 19, Sep 26, November 16, December 10, and 2012 January 22, showing the visual-light echo. In the left two panels, the top and bottom arrows point to echos that appeared in regions N1 and S1 (as defined in Figure 3), respectively. The arrows in the center panel indicate echos that appeared in regions N2, NW, W, and S2 (clockwise from top).

4. Structure of the Remnant and Distance to T Pyx

The most natural interpretation of the variable visual emission from the old remnant around T Pyx is that light emitted by the WD near the peak of the 2011 nova eruption was reflected into our line of sight by dust in the remnant. Numerous pieces of evidence support this interpretation. Using past estimates of T Pyx’s distance of 3.5 ± 1 kpc (Patterson et al. 1998; Schaefer et al. 2010; Shore et al. 2011), the delay between the peak of the direct optical emission and the appearance of the echo was consistent with the light-travel time from the central binary to the remnant. Furthermore, dust exists in the remnant (with a dust-to-gas ratio of approximately 2×10^{-4} by mass; Contini & Prialnik 1997). Additionally, although the remnant was flash ionized (Shara et al. 2013), radiation from recombination did not contribute significantly to the visual echo, as evidenced by: 1) the low level of the Paschen recombination continuum based on a scaling from the $H\alpha$ flux; and 2) our non-detection of any strong recombination lines (e.g., [O I] 5577Å or He I 5876Å) in the spectrum in Figure 2. Our non-detection of echoes in the F225W and FQ422M filters and detection of echoes in the F547M and F600LP filters is consistent with the colors of emission from the central source near optical maximum (see Surina et al. 2013, and assuming gray dust). Finally, the amplitude of fluctuations in brightness of the extended optical light was comparable to that from the central source. We thus refer to the transient, extended visual-band emission as an *echo*.

The delay times between variations in brightness of the central source and those of the various echo patches reveal the geometry of the remnant around T Pyx. Light from the central source reflecting off dust in the remnant travels to us via longer paths than light coming directly from the central source; the difference in arrival times between two photons emitted simultaneously but traveling these different paths — the *delay time*, t — depends upon the reflecting parcel’s location with respect to the illuminating central star. Following

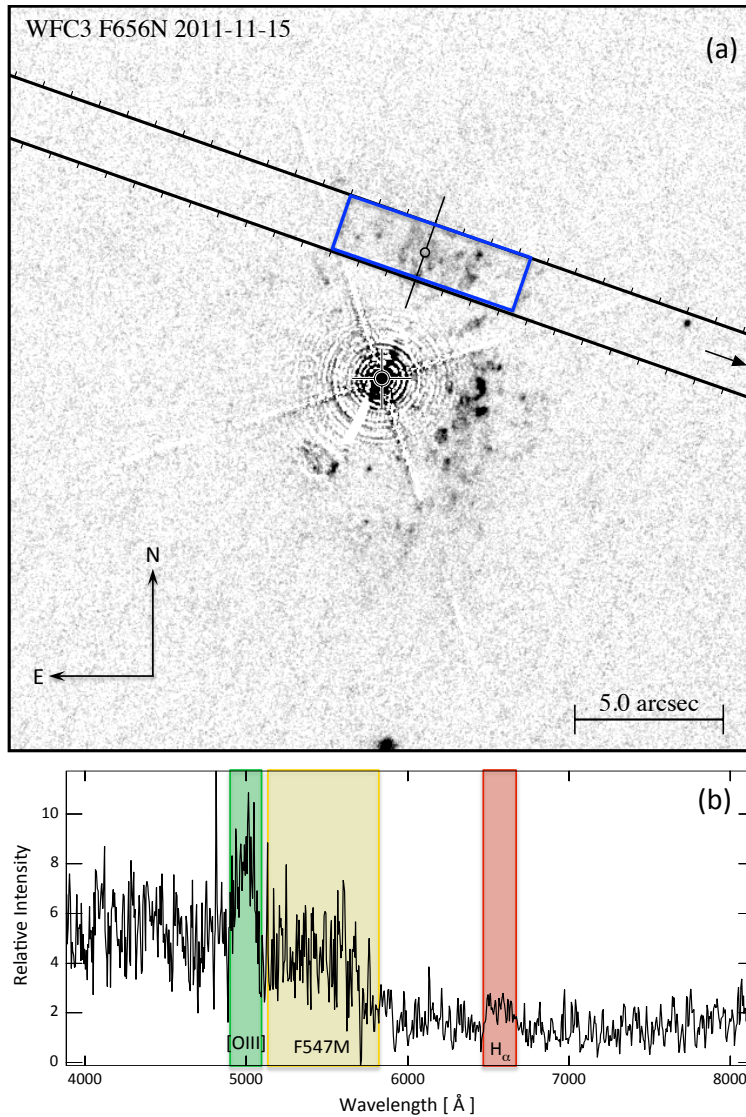


Fig. 2.— STIS spectrum of the echoing remnant. *a)* The position of the slit on 2011 December 5 superimposed on a PSF-subtracted archival WFC3/F656N image from 2011 November 15 (for a description of the WFC3/F656N observations, see Shara et al. 2013). The blue rectangle shows the region of the spectral extraction. *b)* A summed, one-dimensional extraction of the combined G430L and G750L spectra. The left-most rectangle shows the spectral range of diffuse, low-velocity [O III] 5007 emission uniformly filling the slit; the right-most rectangle shows the same for H α emission. STIS detected line emission clearly in [O III] and weakly in H-alpha. The central rectangle shows the FWHM bandpass of the WFC3/F547M filter used in our light-echo analysis; there is no strong line emission in this passband. The echo that we detected is thus consistent with dust-scattered continuum from the outburst.

Couderc (1939), the distance from the WD to the reflecting parcel projected along our line of sight (the *foreground distance*, z) is given by

$$z = \frac{\rho^2}{2ct} - \frac{ct}{2}, \quad (1)$$

where $\rho = \theta D$ is the distance between the central source and reflecting parcel projected onto the plane of the sky (with D the distance from the observer to T Pyx), c is the speed of light, with z measured from the plane of the sky containing the central source *toward* the observer. Table 2 lists the delay times that minimize χ^2 when we model the light curves from the six regions that have the strongest echo signals as shifted versions of the optical light curve from the erupting WD (using V -band observations from the American Association of Variable Star Observers; AAVSO; Henden 2013). Since θ is observable, for a given D the delay times provide the 3-dimensional geometry of the reflecting material. Conversely, if z is known for even a single reflecting parcel, the delay time for that parcel gives D .

Even before we consider the precise delay times, the morphology and progression of the light echo reveals that the principal structure of the remnant around T Pyx is a clumpy ring that is modestly inclined with respect to the plane of the sky. Recognizing that the brightness of the central source did not allow for detection of echoes with delay times of less than about 120 days, the gross motion of the echo across the remnant in a westerly direction demonstrates that foreground distance decreases to the west. The lack of a detectable echo peak from the eastern side of the remnant (region E in Figure 3) after 2011 September is consistent with material on that side producing only reflections with short delay times and therefore having larger foreground distances than material on the western side of the remnant. In addition, although the echo progressed to larger θ (especially in the north and south between 2011 September and December), it did not subsequently move inward, as would be expected if the main reflecting structure had a quasi-spherical shell-like shape.

Table 2. Delay Times and Foreground Distances for Key Echo Regions

Location of Echo Patch ^a	Delay Time ^b (day)	θ^c ($''$)	z^d (10^{17} cm)
north (N1)	125 ± 8	4.52	0.0 ± 0.4
south (S1)	136 ± 5	4.99	0.1 ± 0.4
north #2 (N2)	156 ± 5	5.50	-0.1 ± 0.4
south #2 (S2)	162 ± 3	5.82	0.0 ± 0.4
northwest (NW)	159^{+10}_{-1}	3.99	-1.1 ± 0.2
west (W)	164^{+20}_{-5}	3.32	-1.5 ± 0.2

^aFigure 3 shows the locations of the echo patches.

^bUncertainties correspond to the range of delay times immediately around the optimal t providing acceptable matches between the light curves of the central source and the echo patch.

^c θ is the angular distance between the central binary and the center of light of the echo patch.

^dForeground distances, z , are based upon a distance to T Pyx of 4.8 ± 0.5 kpc.

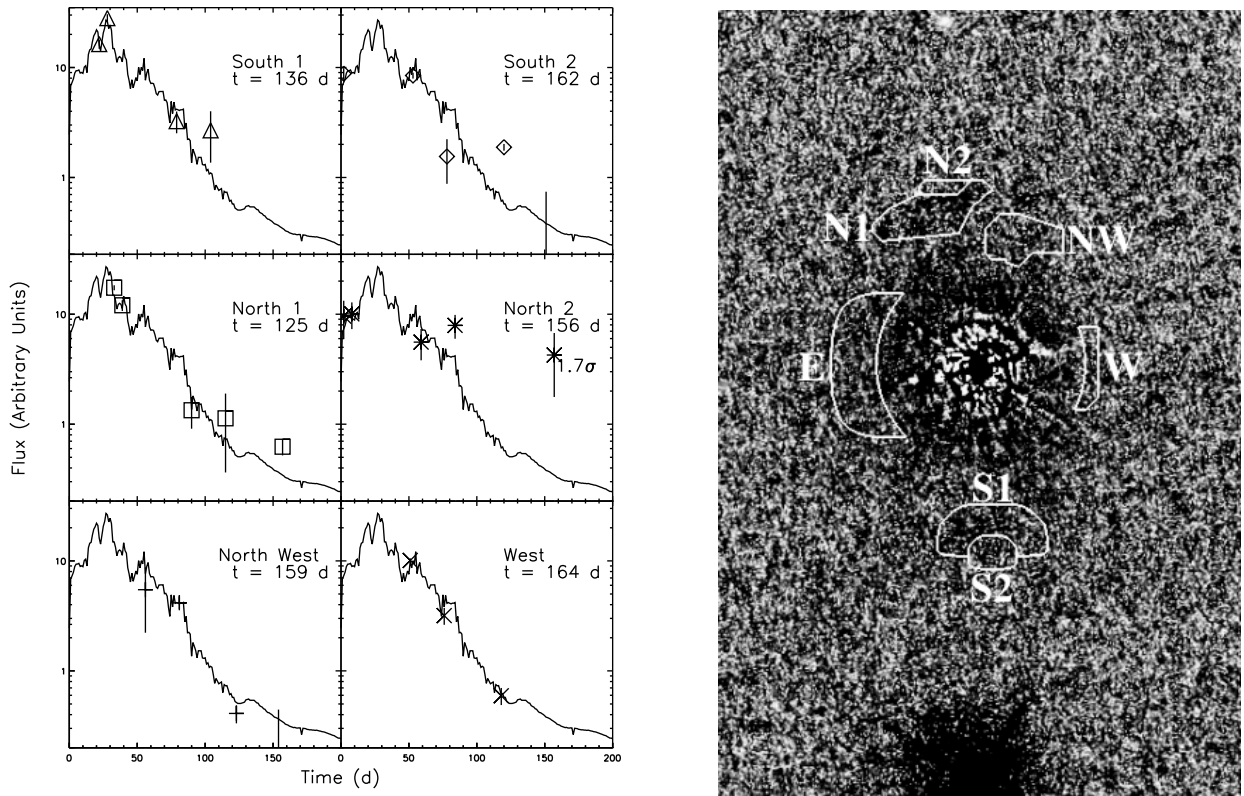


Fig. 3.— *Left panel:* *V*-band light curves of the erupting WD, from the AAVSO (Henden 2013), with visual-band light curves from the six strongest echo regions shifted by the delay times listed in Table 2 and over-plotted. *Right panel:* Extraction regions for the echo light curves, superimposed on the PSF-subtracted WFC3 visual image from 2011 July.

Thus, the more-or-less circular appearance of the known remnant is due not to spherical symmetry, but to a 2D disk-like structure. Moreover, the plane containing this structure is rotated with respect to the plane of the sky around a N-S axis. The consistency between the locations of the echoes and the known remnant indicates that the remnant is the source of the reflecting material, and that this material sits in a ring.

Assuming the binary is coplanar with the ring, the delay times for the echo regions to the north and south of the central binary give the distance to T Pyx. The assumption that the binary is coplanar with the inclined ring is justified on multiple grounds. If the ring was in front of the binary from the point of view of the observer, symmetry arguments suggest that we would expect another ring behind the binary generating an echo at late times. But no such second echo occurred, which rules out values of D larger than 4.8 kpc, derived below. Distances less than 4.8 kpc are disfavored by Shore et al. (2011). Moreover, the ring’s inclination around the N-S axis means that all reflecting clumps to the north and south must have the same z , which only happens for a distance of around 4.8 kpc. With that distance, the central binary does indeed lie near the center of the ring (i.e., $z \approx 0$ for regions N1, N2, S1, and S2). Plugging θ and t for the four echo patches to the north and south of the central binary into Equation 1, we obtain four distinct distance estimates of 4.8, 4.7, 4.9, and 4.8 kpc. Although the dispersion in the distance measurements from the four light-echo patches is nominally just 0.1 kpc, additional uncertainty of $\sim 10\%$ associated with our geometrical assumptions and the complexity of the central-source light curve indicate $D = 4.8 \pm 0.5$ kpc.

The foreground distances to the western and northwestern clumps (see Table 2) give inclination angles for the ring of 30° and 40° , respectively. For comparison, published estimates of the inclination of the central binary range from 6° to about 30° (e.g. Shahbaz et al. 1997; Patterson et al. 1998; Selvelli et al. 2008; Uthas et al. 2010; Patterson et al.

2013).

H α observations with *HST*/F656N (Shara et al. 2013) support our interpretation of the light echo. If the transient H α emission from the remnant was due to recombination following ionization by the UV flash at the start of the eruption, and the visual-band echo was due to dust-scattering of the optical emission that peaked about 30 days into the eruption (as we propose here), we would expect the H α brightening to lead the visual echo by about 30 days. Thus, we expect the maximum angular extent of the H α emission to exceed that of the visual echo at the same observational epoch by $\Delta\theta = (c \Delta t/D) = 1.1'' (D/4.8 \text{ kpc})^{-1} (\Delta t/30 \text{ d})$, where Δt is the difference between the delay times for the H α and visual brightenings, along directions where $z = 0$. Averaging over the northern and southern echo patches in 2011 September, the H α emission described by Shara et al. (2013) is approximately an arcsec more extended in θ than the visual echo (and more to the west) — supporting both the physical mechanism of the echo and our distance estimate. The east-to-west motion of the H α recombination emission, and lack of a connecting arc between the northern and southern H α emission components in 2011 September, are also consistent with the reflecting structure being dominated by a patchy, inclined ring.

5. Implications

The finding of a ring-like component in the remnant around T Pyx, with an inclination comparable to that of the orbital plane of the binary, suggests that the companion helped shape the ejecta. Account for the optical spectra of O’Brien & Cohen (1998), it appears that the ring-like formation that produced the visual echo is part of a three-dimensional shell-like structure. Moreover, using the distance of $4.8 \pm 0.5 \text{ kpc}$, the radial velocity of about 500 km s^{-1} that O’Brien & Cohen (1998) found for material at the back and the

front of the shell is comparable to the expansion speeds in the plane of the sky of many of the knots with θ between about $4''$ and $5''$ (the expansion speeds in the plane of the sky of the fastest, outermost knots are close to $1,000 \text{ km s}^{-1} \{D/4.8 \text{ kpc}\}$; Schaefer et al. 2010). Although the mechanism by which the donor star might shape the remnant is poorly understood, hydrodynamical simulations demonstrate that an orbiting companion can produce rings such as those seen in images of old novae (Lloyd et al. 1997; Porter et al. 1998). Alternatively, we cannot rule out the possibility that at least some of the material in the torus emanated directly from the heated donor star. In T Pyx, the increase in orbital period during quiescence indicates that even between outbursts, the binary blows a strong wind (e.g., Uthas et al. 2010).

A distance to T Pyx of $4.8 \pm 0.5 \text{ kpc}$ means that the quiescent-state accretion rate in this system is inescapably high. The new, more accurate distance also reduces the uncertainties on all of the fundamental parameters of this system. Using this distance, the accretion rate is confirmed to be approximately three orders of magnitude higher than expected for mass transfer driven by gravitational radiation (e.g., Knigge et al. 2000). If such high accretion rates can be stimulated by nova eruptions in close binaries (as suggested by Knigge et al. 2000), and if they can be maintained for even a few decades following an explosion, then novae must strongly impact the evolution of a close binary. By supporting the idea that a nova can catapult a CV into a state of rapid mass transfer, during which the WD can in principle gain mass efficiently (Bours et al. 2013), our confirmation of the large distance and high quiescent-state rate of accretion for T Pyx could have bearing on the problem of how the WDs in CVs can grow to surprisingly large masses (Zorotovic et al. 2011). And although the WD in T Pyx does not appear to be on its way to the Chandrasekhar limit (Patterson et al. 2013; Nelson et al. 2013), its illustration of the phenomenon of nova-stimulated mass transfer could provide a hint about how others CVs might possibly evolve to become type Ia supernovae.

We are grateful to J. Patterson, D. Zurek, C. Knigge, M. Shara, and B. Schaefer for useful discussions. We appreciate STScI's (particularly Tony Roman's) patience with these difficult observations. J.L.S., A.C., and H. U. acknowledge support from grant HST-GO-12448. J.L.S. acknowledges support from NSF award AST-1211778.

Facilities: HST (WFC3, STIS), AAVSO.

REFERENCES

- Bode, M. F., O'Brien, T. J., & Simpson, M. 2004, *ApJ*, 600, L63
- Bond, H., et al. 2003, *Nature*, 422, 405
- Bours, M. C. P., Toonen, S., & Nelemans, G. 2013, *A&A*, 552, 24
- Contini, M., & Prialnik, D. 1997, *ApJ*, 475, 803
- Couderc, P. 1939, *Annales d'Astrophysique*, 2, 271
- Lloyd, H. M., O'Brien, T. J., & Bode, M. F. 1997, *MNRAS*, 284, 137
- Henden, A. A. 2013, Observations from the AAVSO International Database,
<http://www.aavso.org>
- Knigge, Ch., King, A. R., & Patterson, J. 2000, *A&A*, 364, L75
- Nelson, T. 2013, arXiv:1211.3112
- O'Brien, T. J., & Cohen, J. G. 1998, *ApJ*, 498, L59
- Osborne, J. P., et al. 2011, *ATel* # 3549
- Patterson J. et al. 1998, *PASP*, 110, 380
- Patterson, J., et al. 2012, arXiv:1212.5836
- Patterson, J., et al. 2013, arXiv:1303.0736
- Porter, J. M., O'Brien, T. J., & Bode, M. F. 1998, *MNRAS*, 296, 943
- Schaefer, B. E., Pagnotta, A., & Shara, M. M. 2010, *ApJ*, 708, 381
- Selvelli P., Cassatella A., Gilmozzi R., González-Riestra R. 2008, *A&A*, 492, 787

- Shahbaz T., Livio M., Southwell K. A., Charles P. A. 1997, ApJ, 484, 59
- Shara, M. M., Moffat, A. F. J., Williams, R. E., & Cohen, J. G. 1989, ApJ, 337, 720
- Shara, M. M., Zurek, D. R., Williams, R. E., Prialnik, D., Gilmozzi, Moffat, A. F. J. 1997, AJ, 114, 258
- Shara, M. M., et al. 2013, in preparation
- Shore, S. N., Augusteijn, T., Ederoclite, A., & Uthas, H. 2011, A&A, 533, L8
- Slavin, A. J., O'Brien, T. J., & Dunlop, J. S. 1995, MNRAS, 276, 353
- Soker, N., & Tylanda, R. 2007, ASP, 363, 280
- Surina, F., Hounsell, R. A., Bode, M. F., Darnley, M. J., Harman, D. J., & Walter, F. M. 2013, ASP Conf. Series, Stella Novae: Future and Past Decades; arXiv:1303.6592
- Swope, H. H. 1940, Harvard College Obs. Bulletin, 913, 11
- Uthas, H., Knigge, C., & Steeghs, D. 2010, MNRAS, 409, 237
- Waagen, E. 2011, CBET 2700
- Wesson, R., et al. 2008, ApJ, 688, L21
- Zorotovic, M., Schreiber, M. R., & Gänsicke, B. T. 2011, A&A, 536, A42